Multibody Syst Dyn (2015) 35:277–298
DOI 10.1007/s11044-015-9463-x

An enhanced cylindrical contact force model

C. Pereira[1] · A. Ramalho[2] · J. Ambrosio[3]

Received: 10 May 2014 / Accepted: 13 May 2015 / Published online: 17 June 2015

Abstract The penalty formulations that describe the contact forces between different bodies of a mechanical system use the penetration as a representation of the local deformation. The dynamic analysis of the system is conducted assuming explicit or implicit relations between contact force and penetration, dependent on the geometries and material properties of the contacting points. Most of the cylindrical contact force models are based on the Hertz pressure distribution, exhibiting the same restrictions of the Hertz elastic contact theory, which prevent them from being used with conformal contact conditions often observed for low clearances. Furthermore, the existing cylindrical contact models represent the contact force as an implicit function of the penetration with logarithmic expressions, which pose some limitations in their use. We propose an alternative analytical cylindrical contact force model that describes the contact force as an explicit function of the penetration. The new enhanced cylindrical contact force model is based on the Johnson contact model and complementary finite element analysis valid for internal and external cylindrical contact. We show that, within the domain of validity of the Johnson contact force model, the forces predicted with the proposed model are well correlated with reference models, actually expanding their application range. The performance of the proposed model is demonstrated with the analysis of a multibody slider-crank mechanism in which one of the joints exhibits mechanical clearances.

✉ J. Ambrosio
Jorge.ambrosio@tecnico.ulisboa.pt

C. Pereira
candida@isec.pt

A. Ramalho
amilcar.ramalho@dem.uc.pt

1 Dept. of Mechanical Engineering, Polytechnic Institute of Coimbra, R. Pedro Nunes, 3030-199 Coimbra, Portugal

2 Dept. of Mechanical Engineering, University of Coimbra, R. Luis Reis Santos, 3030-788 Coimbra, Portugal

3 LAETA, IDMEC, Instituto Superior Tecnico, University of Lisbon, Av. Rovisco Pais, 1049-001 Lisboa, Portugal

Keywords Cylindrical contact force models · Contact mechanics · Multibody dynamics · Cylindrical contact modeling · Penalty formulation

1 Introduction

Whenever a component in a multibody system experiences impact, forces of a complex nature take place being the corresponding impulse transmitted throughout the chain of bodies of the system, which in turn has a noticeable influence on the dynamic response of mechanical systems. The use of continuous contact force models, as opposite to the discontinuous formulations, has been shown to be suitable and accurate for the treatment contact problems [1–5], in particular, in the presence of multiple impacts, when long contact periods are involved or when frequent intermittent contacts are observed as in many applications of multibody systems [6, 7]. The evolution of the normal contact forces also provides the basis of many friction models required for the dynamic impact analysis of multibody systems [1, 8]. In the process, the information on the contact forces, contact deformation, contact duration, reaction forces, energy dissipation, velocity, and acceleration is continuously available at every time step of the dynamic simulation for all multibody system components fulfilling the input requirements of most engineering design or analysis processes [7, 9–11].

In the continuous contact force method, the occurrence of penetration is used as the basis to evaluate the local deformation of the contacting bodies [1, 3, 12–14]. The dynamic analysis is conducted continuously by explicitly or implicitly assuming a relation between the contact force and penetration, which depends on different types of contacting geometries [1, 14]. For spherical impact geometries, where the contact areas assume a circular or ellipsoidal shape, the contact parameters used to define the continuous contact force are estimated by applying the Hertz elastic contact theory [15, 16]. Unfortunately, for line contact, characterized by rectangular contact areas depicted in Fig. 1 and observed for contact involving cylindrical shape bodies with parallel axis, the physical meaning of contact parameters is not straightforward, and their values are not easily obtained [17]. Current cylindrical contact force models are not only nonlinear, but they represent the contact force as implicit functions of the penetration [18–21]. As a result, when used in the framework of forward dynamic analysis, a numerical iterative technique is required to evaluate the contact force at each integration time step. This is not only computationally costly but also represents a numerical difficulty for the performance of a computational program, especially if a greater number of contacting bodies are involved. Furthermore, due to their mathematical formulations, the range of forces and deformation in which they can be applied are limited [22, 23]. None of the models used for cylindrical contact considers energy dissipation as part of the normal contact force evaluation, which is an important source of damping in practical applications.

Based on the earlier work of Hunt and Crossley [24], Lankarani and Nikravesh [3] propose a contact model where the Hertz contact model [15, 16] is modified by adding a term that accounts for the energy dissipation that occurs during the impact process [3, 24]. Although developed in the framework of point contact, this model has been widely used by many researchers for modeling contact forces in multibody systems for spherical and even for cylindrical contacting geometries [1, 7, 11, 25]. The use of the Lankarani and Nikravesh model indiscriminately for spherical and cylindrical contact, disregarding the different formulation of the proportionality coefficient can only be understood by the fact that in planar multibody systems the formulations of the revolute and spherical joints are the same. However, this confusion is inconsistent with the physical contact phenomena and erroneous.

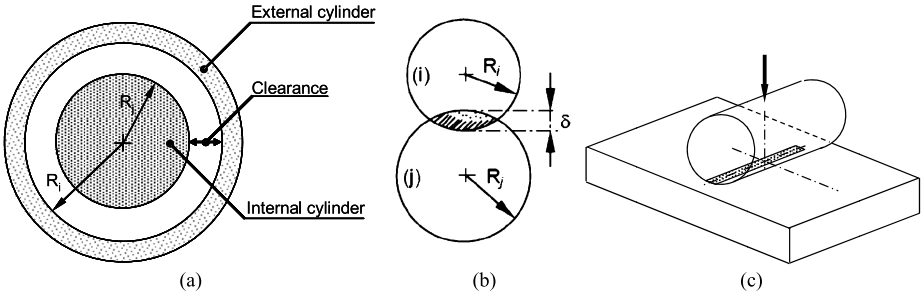

Fig. 1 Dimensional characteristics and definitions for cylindrical contact: (**a**) internal contact; (**b**) external contact; (**c**) shape of contact area

When compared with other analytical cylindrical contact force models, for example, the Johnson model, the Lankarani and Nikravesh contact model [3] is simply a rough approximation to estimate the contact forces between two cylindrical bodies [23].

Based on Winkler elastic foundation, Liu and coworkers [26] proposed a simple and straightforward cylindrical conformal contact model where the contact force is directly calculated from a given penetration. The relations between the contact force and the penetration are obtained by using the Johnson model, the Persson theory, and finite element analysis of cylindrical contact with several clearance values. It is concluded that the Johnson model is effective only when the clearance is large enough and the contact force is small or medium, which implies that it should not be used in conditions of cylindrical conformal contact. In what the Persson theory is concerned, it can be applied only in the case of small clearances and large enough semiangle of contact. However, the validation of the model proposed by Liu and co-workers and of other models is done by using a detailed finite element analysis but for a range of contact conditions, dimensions of contacting cylinders, clearances, penetrations and elastic material properties, specific for the applications is foreseen in each of them [26, 27].

Due to its mathematical formulation and experimental basis, the Johnson model has a specific validity domain, which depends on the clearance value and material properties [23]. The range of contact conditions used by Liu and coworkers is also limited to the specific conditions considered in its formulation, in particular what concerns to penetration values and dimensions of contacting bodies [22]. Many other cylindrical contact models discussed by Pereira et al. [22, 23] have limitations that impair their use in ranges of parameter values required by practical applications. In addition, none of these models accounts for the energy dissipation process that characterizes and conditions many impact phenomena [13, 27, 28].

To overcome the limitations of the current cylindrical models, an analytical model free of mathematical and physical limitations and defining the contact force as an explicit function is a desirable alternative for implementation in a computational code for the dynamic analysis of multibody systems that experience impacts and contacts between cylindrical bodies. With this purpose, we present here a new enhanced cylindrical contact force model that includes a penalty term, or pseudo-stiffness, not dependent on the contact force and that accounts for energy dissipation during the impact process. The validation of the model in the framework of existing models and finite element contact analysis is carried in the process. A slider-crank mechanism with a revolute clearance joint is used to establish a comparative analysis between the dynamic responses of mechanism using different contact force models. In the process, the numerical efficiency associated with different contact modeling

approaches is discussed. In order to represent a more realistic description of contact phenomena, the tangential friction forces are included in the slider-crank multibody model. The importance of different terms associated with the energy dissipation is also observed in a smoother dynamic response of the system characterized by the selection of larger time steps in the numerical integration process.

2 Cylindrical contact models

In a recent study concerning models to represent the contact between cylindrical shaped bodies, it has been concluded that both Johnson and Radzimovski contact force models are able to handle a wide range of relative dimensions and material properties, although they present some mathematical limitations in their application [23]. All other models available in the literature present shortcomings that restrict their range of application, in particular relative to the Johnson model. Not only because the Johnson model is more used than the Radzimovski model and the comparison between them is presented in references [22, 23] without showing any relative superiority between them, but also because the Johnson model is validated experimentally in its original development, the Johnson cylindrical contact model is selected here as the starting point for the development of a new enhanced cylindrical contact model.

The Johnson cylindrical contact model relates the normal contact force with the penetration between two cylinders of radii R_i and R_j with axial length L, with parallel axis, by

$$f_n = \pi L E^* \left[\ln\left(\frac{4\pi L E^* \Delta R}{f_n} \right) - 1 \right]^{-1} \delta, \tag{1}$$

where δ is the penetration, accounting for the contribution of both cylinders, which is assumed to be measured at a point distant enough from the contact point, $E^* = E/2(1-\nu^2)$ is the composite modulus, assuming materials with similar elastic modulus E and Poisson coefficients ν, and $\Delta R = R_i - R_j$, is the radial clearance between the two contacting bodies.

Due to the logarithmic form of the Johnson cylindrical contact model, its range of application is limited to a maximum load, dependent on the size of the clearance and on the material properties, above which the contact force decreases with the increase of penetration [22, 23]. In multibody applications, the Johnson contact model is in the category of penalty contact formulations in which the penetration, calculated directly using the system state variables, is known and used to evaluate the contact force. The solution of the nonlinear Eq. (1) requires a numerical iterative technique such as the Newton–Raphson method that may become computationally expensive. Furthermore, this contact model does not include any energy dissipation, preventing it from being used in applications for which there is impact or large variations on the contact load, as considered in Eq. (1).

The contact model proposed by Lankarani and Nikravesh [3] relates the contact force with penetration and includes energy dissipation as

$$f_n = \frac{4E^*}{3} \left(\frac{R_i R_i}{\Delta R} \right)^{1/2} \delta^n \left[1 + \frac{3(1-c_e^2)}{4} \frac{\dot{\delta}}{\dot{\delta}^{(-)}} \right], \tag{2}$$

where c_e is the restitution coefficient, $\dot{\delta}^{(-)}$ is the relative impact velocity, $\dot{\delta}$ is the actual penetration velocity, and the exponent n is generally 1.5 for metallic materials. This model includes a representation of the energy dissipation very similar to that proposed by Hunt and Crossley [24] and has no mathematical limitations, besides the fact that for low restitution

coefficients, it leads to unrealistic contact forces [2]. Furthermore, it provides the contact force directly from the knowledge of the system variables, that is, it does not require the use of any iterative procedure. The most serious problem with the Lankarani and Nikravesh contact model is that it is not a good representation of cylindrical contact leading to contact forces much lower than those predicted by the Johnson model [23], which is experimentally validated.

From the computational point of view, an efficient contact model is represented by the template provided by the Lankarani and Nikravesh contact model, including energy dissipation, and by the accuracy of the Johnson contact model, that is, the model template has the mathematical form of

$$f_n = K\delta^n \left[1 + \frac{3(1-c_e^2)}{4}\frac{\dot{\delta}}{\dot{\delta}^{(-)}}\right], \tag{3}$$

where the proportionality factor K and the exponent n must be evaluated according to the geometry and materials of the contacting surfaces. Note that the form $f_n = K\delta^n$ is similar to the Hertz elastic contact law, which is valid for a wide range of clearances and material properties and serves as the basis for the derivation of the Johnson model. With this purpose, an alternative analytical model for the contact between cylindrical bodies, without the domain validity limitations of the Johnson model, which defines the contact force as an explicit function of penetration, is presented and applied in this work.

3 Enhanced cylindrical contact force model

3.1 Enhanced cylindrical contact force model development

Due to its accurate representation of the cylindrical contact force, the Johnson contact model is used here as the reference to derive the enhanced cylindrical contact model, in the form described by Eq. (3). The values of the constants K and n are obtained by the best fit approximation of a relation of the type $f_n = K\delta^n$ for a wide range of the cylinder radii R_i and R_j and material properties E and ν. For instance, assuming a clearance value of $\Delta R = 50$ μm and elastic material properties of $E = 207$ GPa and $\nu = 0.3$, the best fit for internal cylindrical contact is $K = 312148$ and $n = 1.2370$, whereas for external cylindrical contact, $K = 44935$ and $n = 1.0935$, for a correlation $R^2 > 0.998$ between the Johnson model and the exponential fit. Figure 2 shows the relation between contact force and penetration for the exponential fit and Johnson contact model for the values referred.

The results provided in Fig. 2 show that contact force relations with very good correlations with the Johnson contact force models can be obtained by identifying the proportionality and exponent parameters of Eq. (3) using exponential fit functions. The question now is to know the relations between the values for K and n and the geometrical and material properties of the cylindrical bodies. For this purpose, consider a range of variation for the clearance of 50 μm $< \Delta R <$ 10 mm for internal contact and 5 mm $< \Delta R <$ 500 mm for external contact, which spans clearances in typical mechanical systems to values associated with other types of cylindrical contact. Furthermore, let the material properties have ranges of variations of $0.1 \leq \nu \leq 0.5$ and 20.7 GPa $< E <$ 10000 GPa, which spans the properties of most of the materials used in mechanical engineering applications from plastics to ceramics.

The correlation between the Johnson and the exponential fitted contact models with different exponent values of n as a function of the cylinder radius and material parameters

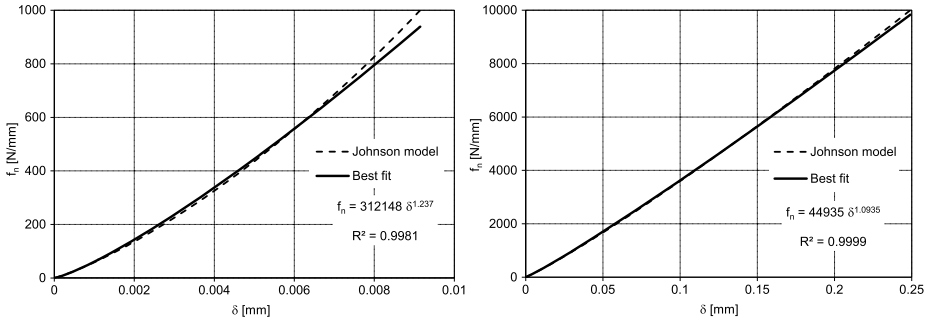

Fig. 2 Best fit of the normal force as a function of the penetration with respect to the Johnson contact model for (**a**) internal contact with $\Delta R = 50$ μm and (**b**) external contact with $\Delta R = 140$ mm, assuming $E = 207$ GPa and $\nu = 0.3$ in both cases

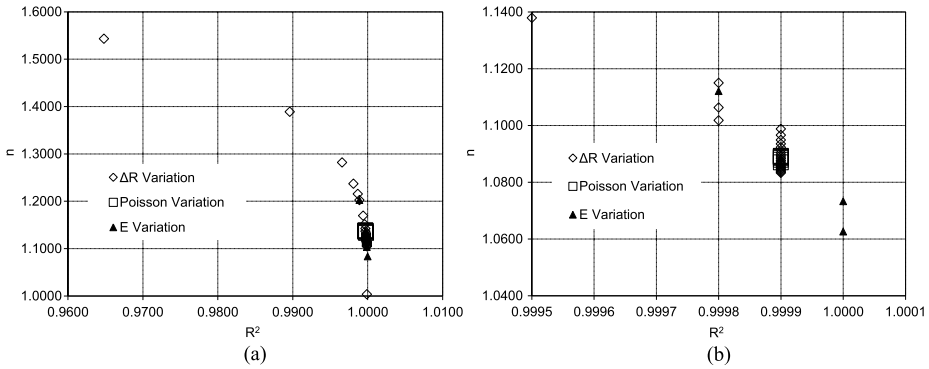

Fig. 3 Variation of the exponent of the exponential for (**a**) internal and (**b**) external cylindrical contact as a function of the variation of the geometry and material

is analyzed. The results shown in Fig. 2 for internal and external cylindrical contacts are obtained for a limited number of values inside the limits of the properties considered.

Figure 3 shows that for internal contacting geometries, the value of the exponent n is quite sensitive to ΔR, whereas it has a much lower sensitivity to the variation of the elastic properties of material. For external contact, the exponent value variation seems to be equally dependent on both ΔR and the elastic modulus. Thus, for internal contact, it is not possible to consider a single value for the exponent n of the contact force model implied in Eq. (3). For external contact, an exponent $n = 1.094$ provides approximations with acceptable correlations for most of the values of the geometric and material properties of the cylinders. Exceptions are observed for the lowest values of ΔR and for the minimum and maximum values of the Young modulus. Therefore, different values of the exponent must be considered in order to guarantee accuracy in the application of the enhanced model in situations with very low clearances.

Although not shown in Fig. 3, the proportionality factor K used in Eq. (3) is also sensitive to the geometric and material properties. An overview of different cylindrical contact force models in general, provided in reference [23], or of the models depicted by Eqs. (1) and (2) suggest some level of proportionality between the contact force and the material constant

E^* and the inverse of the geometric constant $1\backslash\Delta R$. In order to better isolate the effect of the material and geometric constants on the contact force model, we assume that the proportionality factor K in Eq. (3) is given as

$$K = K^* \frac{LE^*}{\Delta R}. \tag{4}$$

Therefore, the constant K^* needs to be identified using the exponential fit function together with the exponential factor n. Furthermore, we assume that K^* and ΔR are linearly related.

The deformations δ are obtained with the Johnson cylindrical contact model for a wide number of combinations of loads, in the range of 10 N/mm $< f_n <$ 1000 N/mm, with material properties in the range of $0.1 \leq \nu \leq 0.5$ and 20.7 GPa $< E <$ 10000 GPa and geometric properties in the range of 50 μm $< \Delta R <$ 10 mm for internal contact and 5 mm $< \Delta R <$ 500 mm for external contact. The combination of different parameter values leads to a collection of deformation-force pairs. With such a collection of results, an optimal problem is defined as the minimization of the deviation between them and those obtained by using the new cylindrical contact model. The parameters of the deformation-force equation of the model are used as design variables, and the optimal problem is solved by using a genetic optimization algorithm [29]. Several runs of the genetic algorithm with different populations and crossovers are attempted in order to obtain better solutions, out of which the best is assumed to be the global minimum, thus providing the best correlation for the enhanced cylindrical contact model.

The best correlation between the Johnson contact model and the new enhanced model is obtained in the form

$$f_n = \frac{(a\Delta R + b)LE^*}{\Delta R} \delta^n \left[1 + \frac{3(1 - c_e^2)}{4} \frac{\dot{\delta}}{\dot{\delta}^{(-)}} \right], \tag{5}$$

where

$$a = \begin{cases} 0.965 & \text{for internal contact,} \\ 0.39 & \text{for external contact,} \end{cases} \tag{6a}$$

$$b = \begin{cases} 0.0965 & \text{for internal contact,} \\ 0.85 & \text{for external contact,} \end{cases} \tag{6b}$$

$$n = \begin{cases} Y\Delta R^{-0.005} & \text{for internal contact,} \\ 1.094 & \text{for external contact.} \end{cases} \tag{6c}$$

In Eq. (6c) the constant Y reflects the fact that for internal contact it is not possible to find a single expression to obtain a good fit, that is, for which a good correlation between the Johnson and exponential fit function for the complete range of clearances ΔR is obtained. The best fit is achieved with the constant Y given by

$$Y = \begin{cases} 1.51[\ln(1000\Delta R)]^{-0.151} & \text{if } \Delta R \in [0.005, 0.34954[\text{ mm,} \\ 0.0151\Delta R + 1.151 & \text{if } \Delta R \in [0.34954, 10.0[\text{ mm.} \end{cases} \tag{6d}$$

Note that $\Delta R = R_i - R_j$ for internal contact and $\Delta R = R_i + R_j$ for internal contact. The remaining quantities in Eq. (5) have the same meaning as in Eq. (1).

3.2 Verification of the enhanced and Johnson models relative to finite element cylindrical contact analysis

In different geometries considered for the finite element analysis of the cylindrical contact, the clearance is defined by changing the radius of the internal cylinder R_i and maintaining

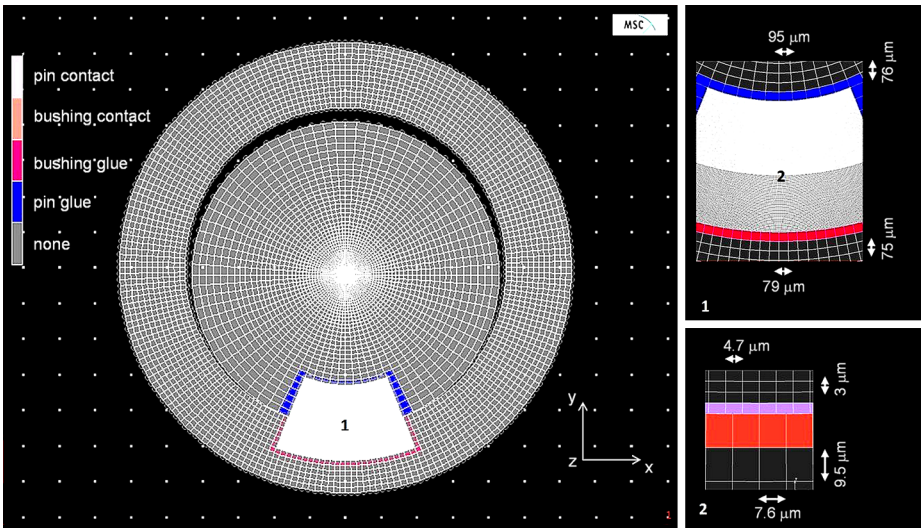

Fig. 4 Deformable/Deformable cylinders' mesh in a contact scenario using MARC®

constant the external cylinder radius $R_j = 2.245$ mm. The cylindrical internal contact is modeled as a deformable/deformable contact, assuming that the internal and external cylinders have equal elastic properties with $E = 2.07 \times 10^{11}$ Pa and $\nu = 0.3$. The mesh geometry, obtained using MARC® nonlinear finite element code, for a clearance value of 0.1 mm, is shown in Fig. 4. The contact definition is introduced in the CONTACT TABLE option described in [28]. The four-node plane stress isoparametric elements used to model the cylinders have sizes between 6.63 and 1.31 μm. The choice of this mesh results from a sensitivity analysis of the contact forces in function of the element sizes that indicates that further mesh refinements do not alter the results obtained [28].

The load is applied in the center nodes of the axis of the internal cylinder. The boundary conditions correspond to fixing upper half of the outside boundary of the external cylinder. The distributions of the contact stress, obtained for clearance values of 1 and 0.01 mm, are shown in Fig. 5. The parabolic shape symmetry of the contact stresses confirms that for this level of clearances, the Hertz elastic contact theory can still be applied.

The penetration values, measured at the internal cylinder center, obtained with the finite element model and those resulting from the application of both analytical contact models, for loads of 20, 40, and 100 N/mm, are evaluated. Figure 6 shows the relation between penetration and clearance for a load of 20 N/mm and clearances values in the range of 5 μm to 1.5 mm. Although not showed here, it must be referred that the same trend observed in Fig. 6 for a load of 40 N/mm is observed for the other loads. The results obtained with the finite element, Johnson, and enhanced contact models differ from each other by less than 10 % in the complete domain of the analysis. For clearances larger than 0.445 mm, the differences are lower than 3 %. The same trend is observed for other levels of loading. Based on these results, we conclude that, even for low clearance values, the Johnson and enhanced cylindrical contact force models provide results with good quality when compared with detailed finite element analysis.

The finite element, Johnson, and enhanced contact models are further verified by a complementary experimental testing campaign reported by Pereira et al. [30]. Such experimental results, although obtained for a limited range of material and geometric conditions, show

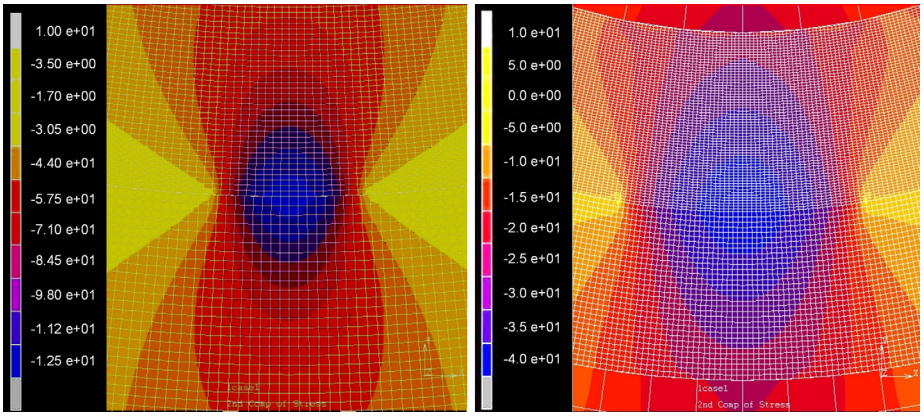

(a) (b)

Fig. 5 Contact stress distributions on the cylinders for clearance values of (**a**) 1 mm and (**b**) 0.01 mm

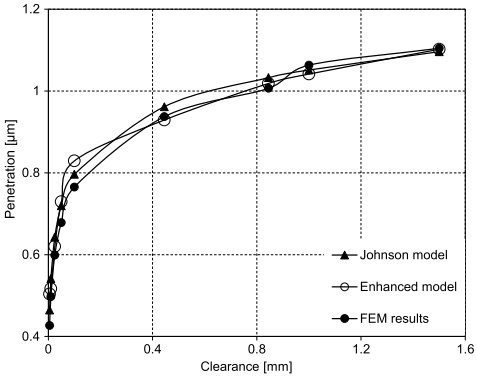

Fig. 6 Comparison of penetration depths obtained with the finite element, Johnson, and the new enhanced contact models

that any of the computational or analytical models considered here provides an accurate description for the cylindrical contact problem.

3.3 Application domain for cylindrical contact models

The practical applications with cylindrical contact are bounded by the limit on the Hertz contact stress that the bodies in contact can exhibit, that is, it cannot exceed the yield stress of the material. For different materials and various clearances, the maximum Hertz stress equals the material yield stress for precise combinations of loads and clearances. The maximum Hertz stress is calculated as [17]

$$\sigma_H = \sqrt{\frac{f_n E^*}{L\pi R}}, \tag{7}$$

where E^*, f_n, and L are the same as defined in Eq. (1), and $R = R_i R_j / \Delta R$. For each material, Fig. 7 shows the maximum contact load that is reached by the material yield stress for different loads, joint clearances, and dimensions of contact bodies. Table 1 summarizes the materials considered and their corresponding elastics properties. Plastic materials are neglected due to their low yield stresses. The range of clearance values from 0.001 mm to

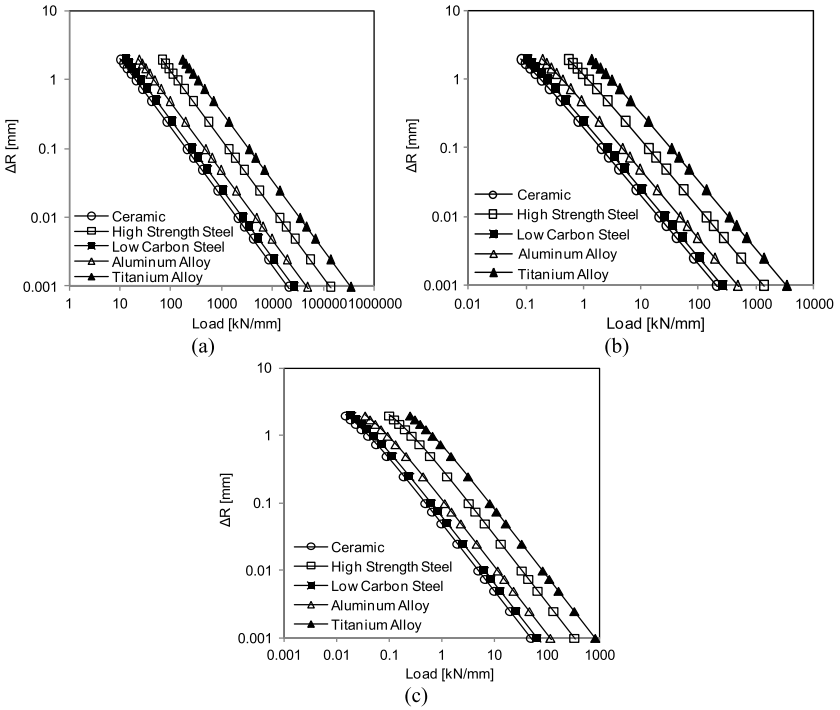

Fig. 7 Combinations between clearance and load leading to a maximum Hertz stress equal to the material yield stress for (**a**) $R_i = 100$ mm, (**b**) $R_i = 10$ mm, and (**c**) $R_i = 5$ mm

Table 1 Types of materials considered and corresponding elastics properties

Type of material	Elastic material properties		
	Young modulus [MPa]	Yield stress [MPa]	Poisson ratio
Ceramic (Tungsten Carbide)	600000	450[a]	0.24
High Strength Steel (DIN 34CrNiMo6)	210000	700	0.30
Low carbon Steel (DIN 1.0402)	200000	300	0.30
Titanium Alloy (DIN Ti6Al4V)	120000	850	0.34
Aluminum Alloy (DIN AlMgSi0.5)	69000	240	0.33

[a]Tensile Strength

2 mm are considered based on the work previously done by the authors, in which the typical ranges of the sets of clearances and loads of the most common applications in mechanical engineering are discussed [22].

It is observed in Fig. 7 that, for a particular material and contact bodies dimension, the range of practical applications involves combinations of clearances and loads that fall be-

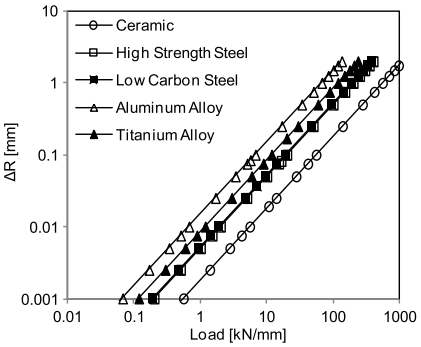

Fig. 8 Combination between clearances that lead to the maximum allowable load in the Johnson contact model for different materials

low the curve in which maximum Hertz stress equals the material yield stress. It must be noted that the variations on the Poisson ratio and Young modulus, associated with different materials, also limit the range of applications for particular values of clearance and loading. Furthermore, the dimension of contact bodies has a greater influence on the limit contact load value that can be applied without reaching plastic deformation. The decrease of the contact area leads to the decrease of the allowable contact load. In what follows, the range of application is defined as the region of a specific graphic for which the maximum Hertz stress is below the material yield stress.

In order to establish a comparative assessment between the enhanced cylindrical model, presented in Sect. 3.1, in relation to the Johnson cylindrical contact force model, the validity domain of the Johnson model must be identified. Thus, to ensure the mathematical and physical meaning of Eq. (1), its logarithmic function must be equal to or greater than 2 [23]. This leads, regardless of contact bodies dimensions, to a load limit value for each clearance value and for each type of material considered given by

$$\ln\left(\frac{4\pi E^* \Delta RL}{f_n}\right) \geq 2 \quad \longrightarrow \quad f_{n\,\mathrm{lim}} \leq \frac{4\pi E^* \Delta RL}{e^2}, \tag{8}$$

where all the symbols have the same meaning as in Eq. (1). The maximum allowable load, which defines the validity domain of the Johnson cylindrical contact force model, is defined by the lines represented in Fig. 8 for the range of clearances and materials under analysis. If the maximum Hertz stresses are evaluated based on the load limits, then the results are, for the different combinations of elastic material properties, clearances, loads, and dimensions of contact bodies, shown by the lines of Fig. 9. The possibility of plastic deformation occurrence increases with the decreasing of contact area dimension and with yield stress value.

3.4 Comparative study of the enhanced and Johnson cylindrical contact models

A comparative assessment of the enhanced and the Johnson cylindrical contact force models is now presented in terms of the differences exhibited by their results and their range of applications. The ranges for this comparative study are 10 N/mm $\leq f_n \leq$ 1000 N/mm for the contact force, 0.0075 mm $\leq \Delta R \leq$ 2 mm for the radial clearance, $0.24 \leq \nu \leq 0.34$ for the Poisson coefficient, and 69 GPa $\leq E \leq$ 600 GPa for the Young modulus. The limit load of 1000 N/mm corresponds to the maximum load per unit of cylinder length, for which the Johnson cylindrical contact model is still valid for the lowest clearance under analysis and for the majority of material types under analysis with the exception of the aluminum

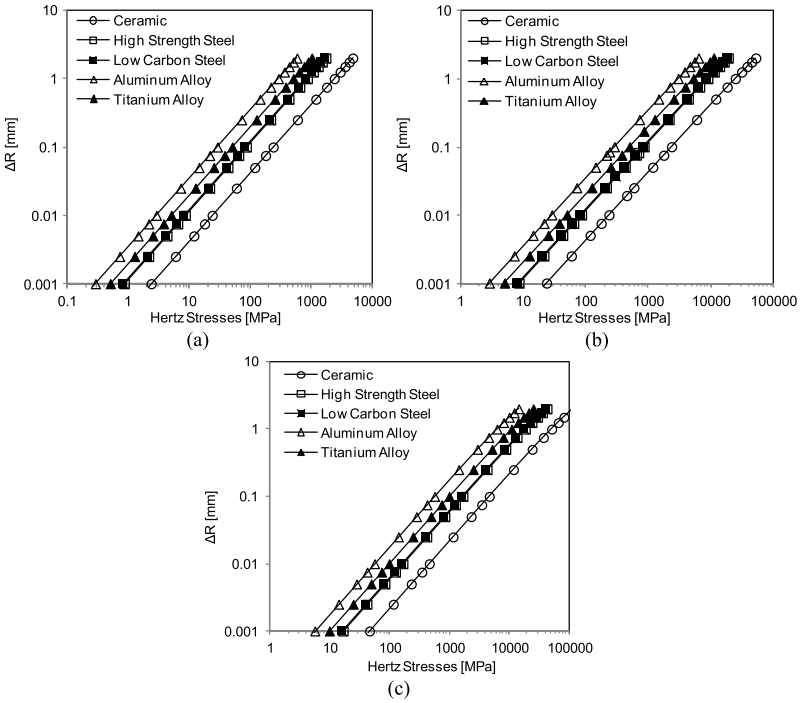

Fig. 9 Combinations between clearance and load leading to the maximum Hertz stress for the maximum allowable Johnson load: (**a**) $R_i = 100$ mm, (**b**) $R_i = 10$ mm, and (**c**) $R_i = 5$ mm

and titanium alloys. For aluminum alloy and clearances of 7.5 and 10 μm, the maximum allowable loads are 494 and 658 N/mm, respectively, beyond which the penetration decreases with increasing load, which is physically inconsistent [23]. For titanium alloy and a clearance of 7.5 μm, the maximum allowable Johnson load is of 865 N/mm. In what follows, the difference between two models is given by

$$Diff_{\mathrm{EM/JM}} = \frac{\delta_{\mathrm{EM}} - \delta_{\mathrm{JM}}}{\delta_{\mathrm{JM}}} 100\ \%, \tag{9}$$

where δ_{EM} and δ_{JM} are penetrations obtained with the enhanced and Johnson cylindrical models, respectively, for combinations of contact load, radial clearance, and material properties.

The maximum differences obtained when the enhanced model is compared with the Johnson model, for the range of ΔR values and loads under analysis, are presented in Figs. 10, 11, 12, 13 and 14 for ceramics, high strength steel, low carbon steel, titanium alloys, and aluminum alloys, respectively. The areas in grey correspond to the combinations of clearance and load for which the difference between the two models is too high due to the impossibility of using the Johnson contact model in such regions. For plastic materials, the comparison between models does not make sense due to the restricted validity domain presented by the Johnson model. From Figs. 10–14 we can conclude that the enhanced model presents a good agreement in relation to the Johnson model with differences lower than 8 % for the range of conditions with practical applications. These differences are, regardless of material properties, lower than 4 % for moderate loads. For clearances around of 25 μm and moderate

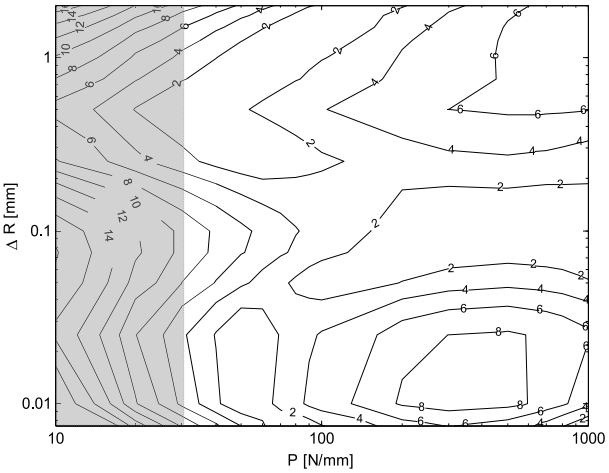

Fig. 10 Differences between the enhanced and Johnson contact models as a function on the variation of the geometry and loading for ceramic ($E = 600$ GPa; $\nu = 0.24$)

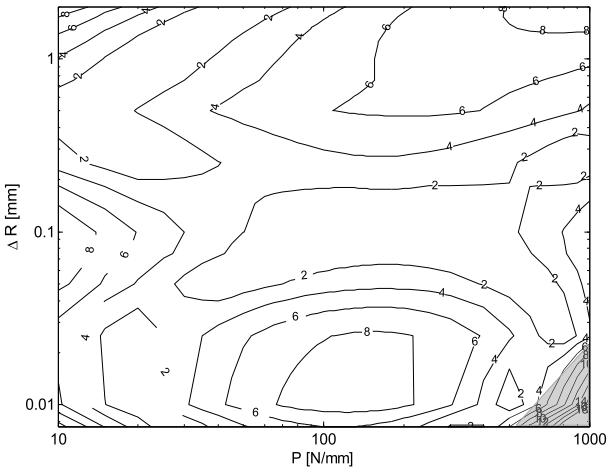

Fig. 11 Differences between the enhanced and Johnson contact models as a function on the variation of the geometry and loading for a high-strength steel ($E = 210$ GPa; $\nu = 0.3$)

loads, a slight increase in the difference is observed, with a maximum value of about 8 %. Nevertheless, in order to cover a wide application domain with a single expression, these differences are acceptable in the limits of the application range.

For the low set of clearances under analysis, an undesirable increase on the difference between models is verified corresponding to high loads. This difference increases with the decreasing of material stiffness. The exception to this behavior is observed for ceramic materials. Combinations of (i) very low clearances and low loads or (ii) high clearances and high loads are contact conditions with no practical applications. The same lack of physical meaning exists in the combinations of (iii) very hard materials with extremely small loads or (iv) low-strength materials and extremely high loads, for example, some aluminum alloys. In these conditions and for current engineering materials, the elastic domain limit of material is quickly reached. The smaller the clearance, the greater the allowable load value that can be applied without reaching plastic deformation, whereas for high clearances, the plastic deformation is quickly reached with increasing loading, as shown in Sect. 3.3. The maximum allowable load increases with the yield strength and the composite modulus of

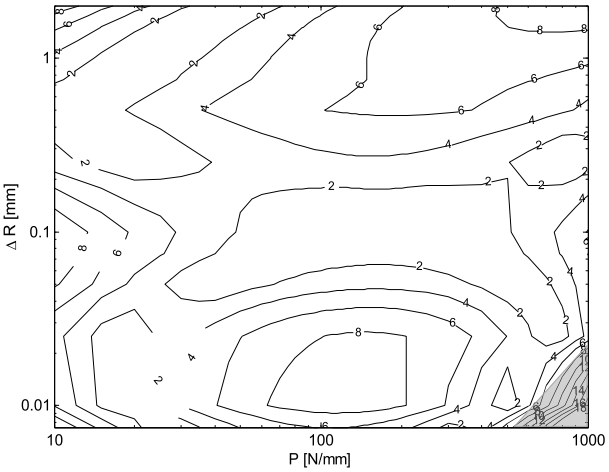

Fig. 12 Differences between the enhanced and Johnson contact models as a function on the variation of the geometry and loading for low-carbon steel ($E = 200$ GPa; $\nu = 0.3$)

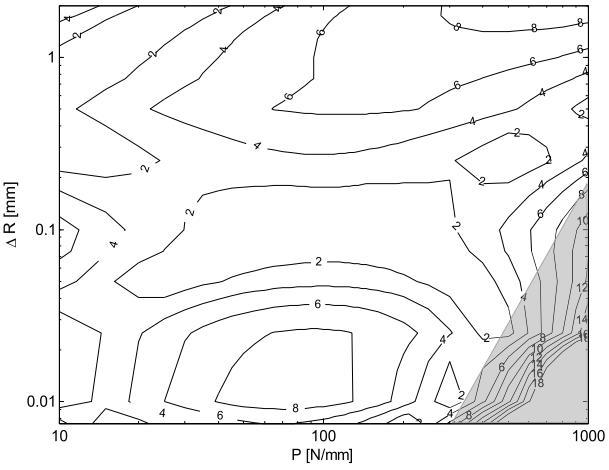

Fig. 13 Differences between the enhanced and Johnson contact models as a function on the variation of the geometry and loading for titanium alloys ($E = 120$ GPa; $\nu = 0.34$)

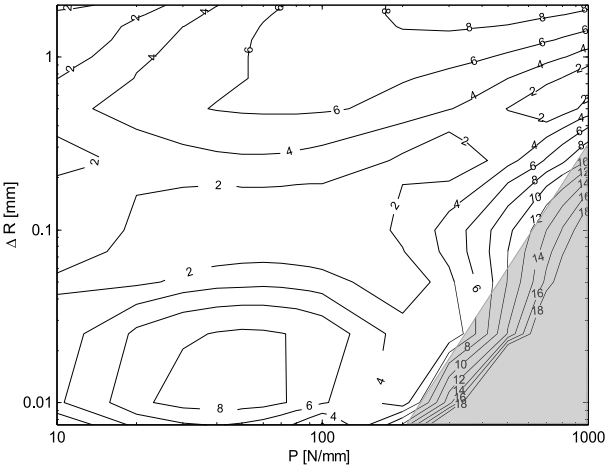

Fig. 14 Differences between the enhanced and Johnson contact models as a function on the variation of the geometry and loading for aluminum alloys ($E = 69$ GPa; $\nu = 0.33$)

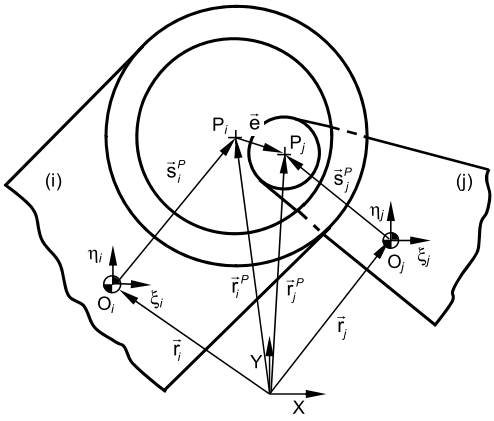

Fig. 15 Generic revolute joint with clearance in a multibody mechanical system [1]

material. For clearance values lower than 0.25 mm and for very high loads, the difference achieved increases, being this increase higher as the material elastic modulus decreases. The limit load that can be applied without reaching plastic deformation decreases with the clearance increase and with the Young modulus decrease.

A similar study can be performed for any other material in which cylindrical contact modeling can be required. The general conclusions on the accuracy of the enhanced model for the materials presented here are also valid for other materials with practical applications; here we do not present such results for the sake of conciseness.

4 Demonstrative application with a slider-crank mechanism

4.1 Multibody systems with clearance joints

To demonstrate the application of the proposed new enhanced cylindrical contact force model, let the equations of motion of a multibody system be formulated using Cartesian coordinates. Let the position and orientation of a generic rigid body i of a multibody system be represented by $\mathbf{q}_i = [\mathbf{r}^T \ \theta]_i^T$, and the position and orientation of all bodies by $\mathbf{q} = [\mathbf{q}_1^T, \mathbf{q}_2^T \ldots \mathbf{q}_{nb}^T]^T$. The equations of motion of a planar multibody system, subjected to holonomic constraints, are [31]

$$\begin{bmatrix} \mathbf{M} & \boldsymbol{\Phi}_\mathbf{q}^T \\ \boldsymbol{\Phi}_\mathbf{q} & \mathbf{0} \end{bmatrix} \begin{Bmatrix} \ddot{\mathbf{q}} \\ \boldsymbol{\lambda} \end{Bmatrix} = \begin{Bmatrix} \mathbf{g} \\ \boldsymbol{\gamma} \end{Bmatrix}, \tag{10}$$

where $\mathbf{M}$ is the system mass matrix, $\boldsymbol{\Phi}_\mathbf{q}$ is the Jacobian matrix associated to the kinematic constraints, $\ddot{\mathbf{q}}$ is the vector that contains the generalized state accelerations, $\boldsymbol{\lambda}$ is a vector of Lagrange multipliers associated to the kinematic constraints, $\boldsymbol{\gamma}$ is a vector with velocity-dependent terms of the kinematic acceleration constraints, and $\mathbf{g}$ is a vector with the forces applied to the rigid body of the system.

For multibody systems in which the kinematic joints exhibit some clearance or flexibility, their contribution to the equations of motion is included in the force vector $\mathbf{g}$, as contact pairs, rather than in the Jacobian matrix $\boldsymbol{\Phi}_\mathbf{q}$ or in the acceleration constraint equations. The clearance revolute joint, illustrated in Fig. 15, is used in the slider-crank mechanism to represent the connection of the slider to the connecting rod. The new enhanced contact force model proposed here is applied in the formulation of this contact pair.

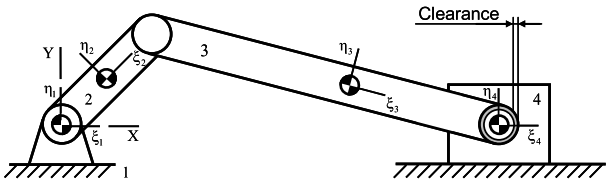

Fig. 16 Slider-crank mechanism with a revolute clearance joint between the connecting rod and the slider

Let body i denote the rigid body that includes the bearing, and body j the one that has the journal of the clearance revolute joint. Let the eccentricity vector $\mathbf{e}$ be defined as

$$\mathbf{e} = \mathbf{r}_i^P - \mathbf{r}_j^P. \tag{11}$$

Contact in the bearing–journal pair will take place if the distance between their centers, evaluated as $\|\mathbf{e}\| = \sqrt{\mathbf{e}^T\mathbf{e}}$, exceeds the allowable clearance, denoted as c. The contact condition is written as

$$\delta = \|\mathbf{e}\| - c \geq 0. \tag{12}$$

When Eq. (12) is fulfilled, the contact forces $\mathbf{f}_i^{(c)}$ and $\mathbf{f}_j^{(c)}$ are applied to the bearing and journal bodies, respectively, at the points of contact. The contact forces are

$$\mathbf{f}_i^{(c)} = -f_n\mathbf{n} + f_t\mathbf{t}, \tag{13a}$$

$$\mathbf{f}_j^{(c)} = -\mathbf{f}_i^{(c)}, \tag{13b}$$

where $\mathbf{n} = [n_x\ n_y]^T = \mathbf{e}/\|\mathbf{e}\|$ is the normal vector to the contact surfaces, and $\mathbf{t} = [n_y\ -n_x]^T$ is the tangential vector.

The normal force f_n is obtained using the enhanced cylindrical contact force model described by Eq. (5). The friction force is described by the Amontons–Coulomb friction force model with the modification proposed in reference [1]

$$f_t = \begin{cases} -c_f c_d f_n \frac{\mathbf{v}_t}{v_t} & \text{if } v_t \neq 0, \\ 0 & \text{if } v_t = 0, \end{cases} \tag{14}$$

where c_f is the friction coefficient, $\mathbf{v}_t$ the relative tangential velocity between the contact surfaces and v_t its magnitude. The dynamic correction coefficient c_d is

$$c_d = \begin{cases} 0 & \text{if } v_t \leq v_0, \\ \frac{v_t - v_0}{v_1 - v_0} & \text{if } v_0 \leq v_t \leq v_1, \\ 1 & \text{if } v_t \geq v_1, \end{cases} \tag{15}$$

where v_0 and v_1 are given preset tolerances for the tangential velocity [1]. For a more detailed description of the formulation of the revolute clearance joint and its computational implementation, the interested reader is referred to [1, 32, 33].

4.2 Slider-crank multibody model

The slider-crank mechanism, illustrated in Fig. 16, is used here to demonstrate the performance of the new enhanced cylindrical contact force model proposed. It has perfect or ideal kinematic joints between all bodies, except for the connection of the slider to the connecting rod that exhibits a clearance.

The geometric and inertia characteristics of the slider-crank mechanism are described in Table 2. In what follows, the crank has an angular velocity of 5000 rpm clockwise, the radius of the bearing of the clearance revolute joint is 10 mm, the journal and bearing axial

Table 2 Geometric and inertia properties of the slider-crank mechanism

Body	Length [m]	Mass [kg]	Moment of Inertia [kg m^2]
2	0.05	0.30	0.00001
3	0.12	0.21	0.00025
4	–	0.14	–

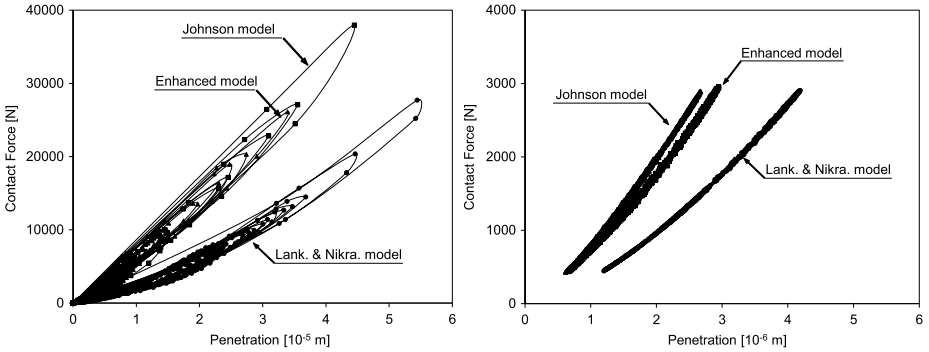

Fig. 17 Contact force vs. penetration depth with a restitution coefficient $c_e = 0.9$ and a clearance of: (**a**) 0.5 mm; (**b**) 0.02 mm

length is 10 mm, and the material properties of the contacting bodies are $E = 207$ GPa and $\nu = 0.3$.

In order to stabilize and keep under control the numerical constraint violations observed during the numerical integration of the equations of motion, the Baumgarte stabilization method [34] is used with $\alpha = \beta = 0.5$. Furthermore, to prevent excessive initial contact penetrations in the contact pairs, the dynamic analysis is carried using a predictor–corrector algorithm, both of variable step size and order [35, 36], for which not only the maximum time step allowed is 10^{-4} s, but also a physical time-step size control, based on the allowable initial penetration during contact, is implemented [37].

4.3 Dynamics of the slider-crank multibody system

In order to understand the consequences of different contact models in the dynamic response of the slider-crank mechanism, the contact between the journal and the bearing is first modeled as being dry and frictionless. Two clearance values of 0.5 mm, typically associated with worn equipment, and 0.02 mm, corresponding to clearance sizes of typical journal–bearing pairs with the dimensions used in this application, are considered here [38]. Figure 17 shows the relation between the contact force and the penetration exhibited by the revolute joint for the Johnson, Lankarani, and Nikravesh and new enhanced contact force models with restitution coefficient $c_e = 0.9$.

In the comparative studies with different contact force models, the contact force model proposed by Lankarani and Nikravesh always leads to softer contact. This is expected because this contact model is based on spherical contact, whereas other models use the cylindrical geometry of the contact pair to define their stiffness. The new enhanced contact force and Johnson models exhibit comparable stiffness in the range of the applications considered.

For larger clearance values, the Johnson contact force model is slightly stiffer than the new enhanced model, the situation being reversed for small clearance values.

The trajectories of the bearing with respect to the journal are depicted in Figs. 18 and 19 for different contact force models and for the clearance values of 0.5 and 0.02 mm, respectively. The relative penetration depth between the journal and bearing is visible by the points of the journal center trajectory that are plotted outside the clearance circle, which is represented by the smooth curves. When no energy dissipation is considered in the normal contact, that is, when $c_e = 1$, all contact models predict shorter contact periods and longer free flight trajectories for larger clearance values. The same behavior has been observed by Pereira et al. when using other contact models such as Dubowsky and Fraudenstein, Goldsmith, or the ESDU-78055 [20, 21]. As a result of short periods of time in which the journal seats in the bearing combined with the higher values of contact forces associated, in particular for cylindrical contact models, a much faster dynamic response can be expected, leading to higher computational costs on its evaluation due to the smaller time steps required to integrate the equations of motion. Otherwise, even when a low energy dissipation is considered in the normal contact, in this case $c_e = 0.9$, most of the trajectories present the pairs in continuous contact. Similar behaviors are reported by other authors [1, 39].

When the friction force is added, in this case with a coefficient of $\mu = 0.1$, the trajectories of the journal with respect to the bearings become mostly in the contact mode. This behavior is more evident for the Lankarani and Nikravesh spherical contact model since the larger penetrations obtained during contact are consistent with its lower stiffness. For cylindrical contact models, some free-flight modes are observed, although with a reduced frequency than that observed when the friction is neglected. This is due to the fact that the cylindrical models lead to a lower penetration depth leading and, in turn, to higher contact forces. Even with the reduction on the global contact force values, due to the friction effect, higher contact forces are achieved when the cylindrical contact models are used. It must also be noticed that when the friction force is accounted for the frequency contents of the dynamic response of the system decrease, the time steps selected by the variable time-step numerical integrator also increase.

Figure 19 demonstrates that when the clearance size decreases, the dynamic behavior tends to be smoother, which is represented by a smaller number of impacts observed and by the long periods of contact, in which the journal follows the bearing wall, that is, that the journal is in permanent contact with the bearing. Nevertheless, the differences between the spherical and cylindrical models are also observed here, with the Lankarani and Nikravesh model leading to higher penetrations in comparison to those reached with cylindrical models.

A common trend among all cases with different clearance and energy dissipation terms and restitution and friction coefficients is that the integration time step selected by the predictor–corrector integration scheme increases with the energy dissipation modeled and with the decrease of the clearance size. No other particular difference in the dynamic behavior of the slider-crank mechanism is observed when using the Johnson or the proposed new enhanced contact force models, as is evidenced particularly by Fig. 18.

5 Conclusions

To overcome the drawbacks presented by the analytical models available in the literature to describe the contact between cylindrical geometries, we have proposed a new enhanced analytical model and discussed its validation. A verification procedure involving finite elements

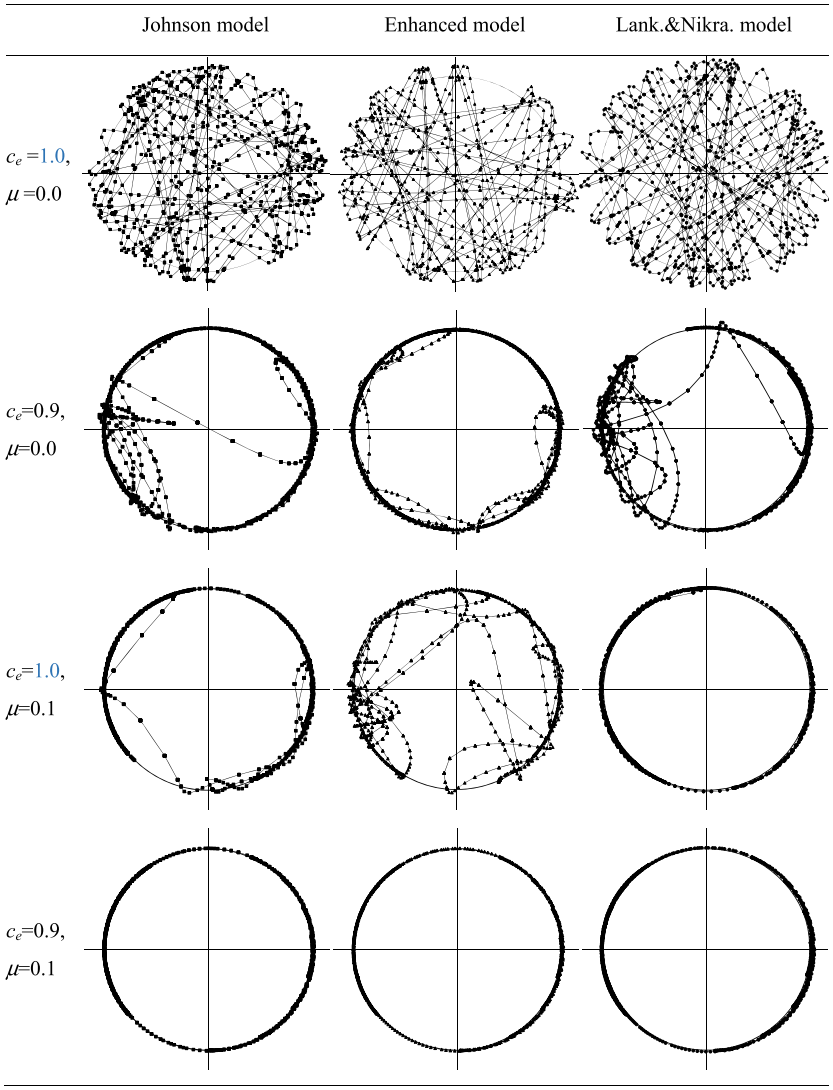

Fig. 18 Journal center trajectory with respect to the bearing using the Johnson, new enhanced, and Lankarani and Nikravesh contact force models with a clearance value of 0.5 mm considering the existence of normal contact energy dissipation and friction

and different cylindrical contact force models was pursued. The results revealed that, for the range of practical applications, in mechanical engineering, in which all model parameter are varied under moderate load values, maximum differences lower than 10 % separate these analytical models. The new enhanced contact model not only has a range of applications that exceeds that of the Johnson contact model but also has a simple and straightforward computer implementation that allows calculating the normal contact force by knowing the penetration that is penalized without using any iterative procedure.

The ability of the new approach to modeling internal cylindrical contact in comparison to other models is demonstrated through the dynamic analysis of a revolute joint with clearance

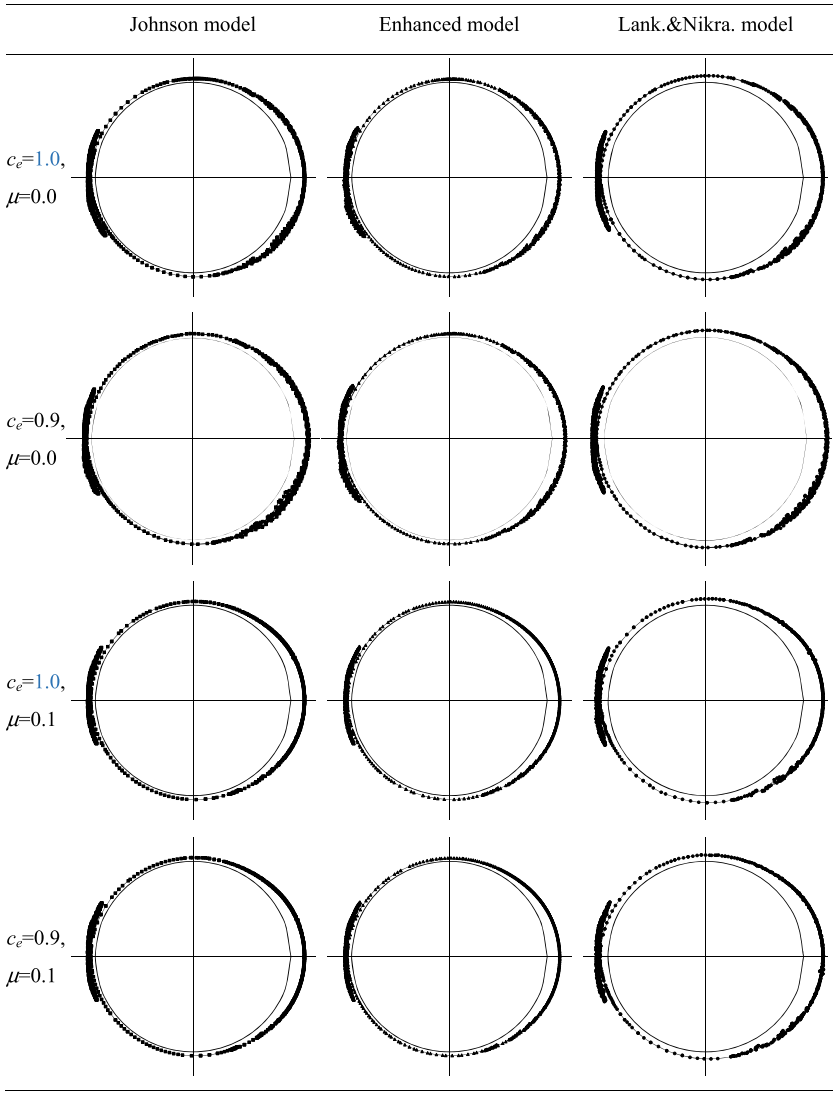

Fig. 19 Journal center trajectory with respect to the bearing using the Johnson, new enhanced, and Lankarani and Nikravesh contact force models with a clearance value of 0.02 mm considering the existence of normal contact energy dissipation and friction

of a slider-crank mechanism. Several simulations demonstrate how different contact force models may influence the dynamic behavior and what the consequences are in terms of contact forces, penetration depths, and journal trajectories. We have demonstrated that the use of spherical models to describe the contact between cylindrical geometries leads to a rough approximation since contact forces are underestimated as a consequence of the softer force-penetration relation that characterizes these models, which do not account for the axial length of the contacting cylinders. It is also demonstrated that when the system components flexibility is not account for and the models are applied as purely elastic models neglecting the system energy dissipation, large contact forces are obtained. As a result, the trajectories

of the journal inside the bearing are characterized by a prevalence of the free-flight modes, instead of contact modes, which does not help the smoothness of the dynamic response of the system, leading to much higher computational costs on its evaluation due to the smaller time steps required to integrate the equations of motion. However, when the friction forces are included, the trajectories of the journal with respect to the bearing become mostly in the contact mode. This implies the decrease of the frequency contents of the dynamic response of the system allowing for the increase of the time steps required by the numerical integrator.

References

1. Flores, P., Ambrósio, J., Pimenta, C.J.C., Lankarani, H.M.: Kinematics and Dynamics of Multibody Systems with Imperfect Joints: Models and Case Studies. Springer, Berlin (2008)
2. Flores, P., Leine, R., Glocker, R.: Modeling and analysis of planar rigid multibody systems with translational clearance joints based on the non-smooth dynamics approach. Multibody Syst. Dyn. **23**, 165–190 (2010)
3. Lankarani, H.M., Nikravesh, P.E.: Continuous contact force models for impact analysis in multibody systems. Nonlinear Dyn. **5**, 193–207 (1994)
4. Zhang, H., Brogliato, B., Liu, C.: Dynamics of planar rocking-blocks with Coulomb friction and unilateral constraints: comparisons between experimental and numerical data. Multibody Syst. Dyn. **32**(1), 1–26 (2014). doi:10.1007/s1044-013-9356-9
5. Zhuang, F., Wang, Q.: Modeling and simulation of the nonsmooth planar rigid multibody systems with frictional translational joints. Multibody Syst. Dyn. **29**(4), 403–423 (2013)
6. Xu, L.-X., Li, Y.-G.: Modeling of a deep-groove ball bearing with waviness defects in planar multibody system. Multibody Syst. Dyn. **33**(3), 229–258 (2015). doi:10.1007/s1044-014-9413-z
7. Pedersen, S.L., Hansen, J.M., Ambrósio, J.: A roller chain drive model including contact with guide-bars. Multibody Syst. Dyn. **12**, 285–301 (2004)
8. Lankarani, H.M.: A Poisson-based formulation for frictional impact analysis of multibody mechanical systems with open or closed kinematic chains. J. Mech. Des. **122**, 489–497 (2000)
9. Tian, Q., Liu, C., Machado, M., Flores, P.: A new model for dry and lubricated cylindrical joints with clearance in spatial flexible multibody systems. Nonlinear Dyn. **64**(1–2), 25–47 (2011)
10. Haines, R.S.: Survey: 2-dimensional motion and impact at revolute joints. Mech. Mach. Theory **15**, 361–370 (1980)
11. Hippmann, G., Arnold, M., Schittenhelm, M.: Efficient simulation of bush and roller chain drives. In: Goicolea, J.M., Cuadrado, J., García Orden, J.C. (eds.) Proceedings of the Multibody Dynamics 2005, ECCOMAS Thematic Conference, Madrid, Spain (2005)
12. Gummer, A., Sauer, B.: Modeling planar slider-crank mechanisms with clearance joints in RecurDyn. Multibody Syst. Dyn. **31**(2), 127–145 (2014)
13. Flores, P., Ambrósio, J., Claro, J.C.P.: Dynamic analysis for planar multibody mechanical systems with lubricated joints. Multibody Syst. Dyn. **12**, 47–74 (2004)
14. Gilardi, G., Sharf, I.: Literature survey of contact dynamics modeling. Mech. Mach. Theory **37**, 1213–1239 (2002)
15. Hertz, H.: On the contact of solids-on the contact of rigid elastic solids and on hardness. In: Miscellaneous Papers, pp. 146–183. Macmillan and Co., London (1896). (Translated by D.E. Jones and G.A Schott)
16. Johnson, K.L.: One hundred years of Hertz contact. Proc. Inst. Mech. Eng. **196**, 363–378 (1982)
17. Harris, T., Kotzalas, M.: Essential Concepts of Bearing Technology. CRC Press, Boca Raton (2007)
18. Radzimovsky, E.I.: Stress distribution and strength conditions of two rolling cylinders pressed together. Eng. Exp. Sta. Univ. Ill. Bull. **408** (1953)
19. Young, W.R., Budynas, R.G.: Roark's Formulas for Stress & Strain. McGraw-Hill, New York (1989)
20. Goldsmith, W.: Impact, The Theory and Physical Behaviour of Colliding Solids. Edward Arnold, Sevenoaks (1960)
21. ESDU 78035 Tribology Series: Contact Phenomena. I: Stresses, Deflections and Contact Dimensions For Normally Loaded Unlubricated Elastic Components Engineering Sciences Data Unit, London (1978)
22. Pereira, C.M., Ramalho, A.R., Ambrósio, J.: A critical overview of internal and external cylinder contact force models. Nonlinear Dyn. **63**, 681–697 (2011)
23. Pereira, C., Ramalho, A., Ambrosio, J.: Applicability domain of internal cylindrical contact force models. Mech. Mach. Theory **78**, 141–157 (2014)

24. Hunt, K.H., Crossley, F.R.E.: Coefficient of restitution interpreted as damping in vibroimpact. Int. J. Appl. Mech. **7**, 440–445 (1975)
25. Machado, M., Moreira, P., Flores, P., Lankarani, H.M.: Compliant contact force models in multibody dynamics: evolution of the Hertz contact theory. Mech. Mach. Theory **53**, 99–121 (2012)
26. Liu, C.-S., Zhang, K., Yang, L.: The FEM analysis and approximate model for cylindrical joints with clearances. Mech. Mach. Theory **42**(2), 183–197 (2007)
27. Lim, C.T., Stronge, W.J.: Oblique elastic-plastic impact between rough cylinders in plane strain. Int. J. Eng. Sci. **37**, 97–122 (1999)
28. Pereira, C., Ramalho, A., Ambrósio, J.: Conformal cylindrical contact force model verification using a finite element analysis. In: Topping, B.H.V., Tsompanakis, Y. (eds.) Proceedings of the Thirteenth International Conference on Civil, Structural and Environmental Engineering Computing. Civil-Comp Press, Stirlingshire (2011), Paper 135
29. Deb, K.: Multi-Objective Optimization Using Evolutionary Algorithms. Wiley, New York (2001)
30. Pereira, C., Ramalho, A., Ambrósio, J.: Experimental and numerical validation of an enhanced cylindrical contact force model. In: de Hosson, J.T.M., Brebbia, C.A. (eds.) Surface Effects and Contact Mechanics X—Computational Methods and Experiments, vol. 7, pp. 49–60 (2011)
31. Nikravesh, P.: Computer-Aided Analysis of Mechanical Systems. Prentice-Hall, Englewood-Cliffs (1988)
32. Zheng, E., ZhouLoad, X.: Modeling and simulation of flexible slider-crank mechanism with clearance for a closed high speed press system. Mech. Mach. Theory **74**, 10–30 (2014)
33. Flores, P., Koshy, C.S., Lankarani, H.M., Ambrósio, J., Claro, J.C.P.: Numerical and experimental investigation on multibody systems with revolute clearance joints. Nonlinear Dyn. **65**, 383–398 (2011)
34. Baumgarte, J.: Stabilization of constraints and integrals of motion in dynamical systems. Comput. Methods Appl. Mech. **1**, 1–16 (1972)
35. Shampine, L., Gordon, M.: Computer Solution of Ordinary Differential Equations: The Initial Value Problem. Freeman, San Francisco (1975)
36. Schoeder, S., Ulbrich, H.: Thorsten Schindler, Discussion of the Gear–Gupta–Leimkuhler method for impacting mechanical systems. Multibody Syst. Dyn. **31**(4), 477–495 (2014)
37. Flores, P., Ambrósio, J.: On the contact detection for contact-impact analysis in multibody systems. Multibody Syst. Dyn. **24**(1), 103–122 (2010)
38. ESDU—65007 Tribology Series: General Guide to the Choice of Journal Bearing Type. Engineering Sciences Data Unit, London (1965)
39. Schwab, A.L., Meijaard, J.P., Meijers, P.: A comparison of revolute joint clearance models in the dynamic analysis of rigid and elastic mechanical systems. Mech. Mach. Theory **37**, 895–913 (2002)